



**HAL**  
open science

## A DfT Strategy for Detecting Emerging Faults in RRAMs

Thiago Santos Copetti, Tobias Gemmeke, Leticia Poehls

► **To cite this version:**

Thiago Santos Copetti, Tobias Gemmeke, Leticia Poehls. A DfT Strategy for Detecting Emerging Faults in RRAMs. 29th IFIP/IEEE International Conference on Very Large Scale Integration - System on a Chip (VLSI-SoC), Oct 2021, Singapore, Singapore. pp.93-111, 10.1007/978-3-031-16818-5\_5. hal-04419565

**HAL Id: hal-04419565**

**<https://inria.hal.science/hal-04419565v1>**

Submitted on 26 Jan 2024

**HAL** is a multi-disciplinary open access archive for the deposit and dissemination of scientific research documents, whether they are published or not. The documents may come from teaching and research institutions in France or abroad, or from public or private research centers.

L'archive ouverte pluridisciplinaire **HAL**, est destinée au dépôt et à la diffusion de documents scientifiques de niveau recherche, publiés ou non, émanant des établissements d'enseignement et de recherche français ou étrangers, des laboratoires publics ou privés.



Distributed under a Creative Commons Attribution 4.0 International License



This document is the original author manuscript of a paper submitted to an IFIP conference proceedings or other IFIP publication by Springer Nature. As such, there may be some differences in the official published version of the paper. Such differences, if any, are usually due to reformatting during preparation for publication or minor corrections made by the author(s) during final proofreading of the publication manuscript.

# A DfT Strategy for Detecting Emerging Faults in RRAMs

T. S. Copetti, T. Gemmeke, and L. M. Bolzani Poehls

*Chair of Integrated Digital Systems and Circuit Design - IDS  
RWTH Aachen University, Germany*

*[copetti, gemmeke, poehls]@ids.rwth - aachen.de,  
WWW home page: <https://www.ids.rwth-aachen.de/>*

**Abstract.** Limitations on Complementary Metal Oxide Semiconductor (CMOS) technology scaling combined with the increasing demand for emerging applications requiring high computing and storage capabilities pose significant challenges to device technologies and computer architectures. From the point of view of device technology, memristive devices have become the most promising candidate to complement and/or replace CMOS technology. The key advantages are the memristive device's CMOS manufacturing process compatibility, zero standby power consumption, high scalability and density, as well as the memristive device's capability to implement high-density memories as well as new computing paradigms. Despite all these advantages, these novel devices are also susceptible to manufacturing deviations that may cause faulty behaviors not observed in CMOS technology, significantly increasing the test complexity. In such context, this paper presents a Design-for-Testability (DfT) strategy able to detect traditional as well as unique faults in Resistive Random Access Memories (RRAMs). In more detail, an on-chip sensor able to perform electrical measurements, while performing a predefined operating sequence, was implemented using an X-Fab technology library. The obtained results demonstrate the proposed strategy's capability to detect unique faults in RRAM cells. Finally, the paper provides a discussion about introduced overheads and implementation granularity.

**Keywords:** RRAMs, DfT Strategy, Traditional Faults, Unique Faults

## 1 Introduction

Over the last fifty years, Moore's and Dennard's laws dictated the CMOS technology miniaturization rate [1,2]. Limitations on the continued transistor scaling and the increasing demand for emerging applications, requiring high-performance systems with strict constraints, pose significant challenges to device technologies and computer architectures. Device technology faces the following three walls, preventing further transistor scaling [3, 4]: (a) the reliability wall - associated with a failure rate increase and lifetime reduction; (b) the leakage wall - meaning that the static power consumption becomes even more important than the dynamic power consumption when considering the overall power consumption,

and (c) the cost wall - showing that the cost per transistor via pure geometric scaling is plateauing, with no tendency to get cheaper. From the computer architecture point of view, the following walls can be identified: (a) the memory wall - due to the limited memory bandwidth that impacts performance and energy consumption of data-intensive applications as well as the growing gap between memory and processor speeds; (b) the power wall - as the practical power limit for cooling is reached and consequently, there is no possibility to further increase the CPU clock frequency; and (c) the Instruction Level Parallelism (ILP) wall - related to the always increasing complexity of keeping all cores running in parallel. These aspects limit the use of CMOS technology and von Neumann architectures as solutions for emerging applications' implementation and increase the necessity for novel devices and architectures. Memristive devices represent one of the most promising candidates to complement and/or replace CMOS technology mainly due to their CMOS manufacturing process compatibility, zero standby power consumption, as well as high scalability and density [4]. However, the fabrication of memristive devices is prone to manufacture deviations, including process variation and manufacturing defects, that can result in faults [5]. A fault is defined as any deviation from the memristor's expected behavior due to process variations, manufacturing defects, or design-induced anomalies [5]. The fault size is related to the deviation's magnitude and can be categorized into three different classes. A deviation higher than the tolerance limit is classified as catastrophic. However, if the deviation only degrades the performance, it is categorized as parametric. Finally, if the deviation's magnitude is insignificant, the fault is called benign. Thus, the use of these novel devices depends on being able to guarantee their proper behavior after manufacturing. Memristive devices are usually integrated during the CMOS Back-End-Of-Line (BEOL) manufacturing process. In this context, it becomes mandatory to properly test the fabricated devices after manufacturing, which requires accurate fault models derived from realistic manufacturing defects. In [6], the authors provide a review of the memristive device manufacturing process as well as a discussion related to the possible defects that may affect these novel devices, identifying the relation between manufacturing failure mechanisms and faulty behaviors. Literature shows that Resistive Random Access Memory (RRAM) cells can be affected not only by traditional faults, but also by unique faults [6–9], demanding the development of new manufacturing test procedures able to properly detect these faults [10,11]. In the last few years, some strategies were proposed in order to test memristor-based circuits. A fault model and two Design-for-Testability (DfT) schemes for RRAMs are presented in [7]. The DfT schemes exploit the access time duration and supply voltage level of RRAM cells to facilitate the detection of unique faults. Moreover, the traditional March Tests that explore the execution of predefined read and write operations applied at each RRAM cell are extremely time-consuming and are also not able to guarantee the detection of all unique faults. In [12] the authors presented a scheme based on "sneak-path sensing" able to test multiple elements of Phase Change Memories (PCM) at the same time (1R RRAM cells). The detection is based on a comparison between

the output current related to a specific group of cells and the ideal current. The groups are accessed based on the execution of March elements. The main drawback of this scheme is related to the fact that it only works for RRAMs that have sneak-paths as well as the fact that the amount of cells that can be tested in parallel is limited.

In such context, this paper proposes a DfT strategy based on the introduction of an on-chip sensor able to perform electrical measurements, while performing a predefined operating sequence to detect both traditional and unique faults in RRAMs. Note that this paper extends the work described in [13]. In more detail, this paper presents an optimized version of the on-chip sensor proposed in [13], making the DfT strategy able to detect all unique faults that can affect RRAM cells. The validation of the proposed strategy was performed using a 1T1R RRAM cell implemented using a 350 nm X-Fab technology library and a memristive model described in [14]. A defect injection scheme based on the introduction of resistors on the 1T1R RRAM cell was adopted. The obtained results demonstrated that the proposed approach is able to detect traditional and unique faults. Finally, the paper also provides a more complete analysis and discussion about introduced overheads and possible implementation granularity when considering a crossbar memory array.

## 2 Background

This Section presents concepts related to memristive devices as well as existing fault models associated to these novel devices.

### 2.1 Memristive Devices

In 1971, Leon Chua postulated the fourth basic circuit element named memristive device, or memristor, while trying to establish a missing constitutive relationship between electrical charge and magnetic flux [15]. A memristive device is a passive element that can be described by the time integral of the current (charge  $q$ ) through the time integral of the voltage (flux  $\phi$ ) across its two terminals [15]. The memristive device has at least two distinct states, the High Resistance State (HRS) and the Low Resistance State (LRS), and can switch from HRS (LRS) to LRS (HRS) by applying a voltage  $V_{SET}$  ( $V_{RESET}$ ) with an absolute value larger than its threshold voltage ( $V_{th}$ ). The essential fingerprint of memristive devices is the pinched current-voltage (I-V) hysteresis loop, illustrated in Fig. 1(a). Note that when the memristive device is floating, or when the voltage  $v(t)$  across the device is zero, the current  $i(t)$  is also zero [16]. An RRAM data storage element is a three-layer device consisting of a dielectric sandwiched between two metal electrodes. In more detail, the memory cell is based on Metal/Insulator/Metal (MIM) structure [17]. The “M” in MIM denotes any reasonably good electron conductor, often asymmetric for the two sides with respect to the materials’ work function and oxygen affinity, while “I” stands for insulator, often an ion or mixed conducting oxide or higher chalcogenide. Fig.

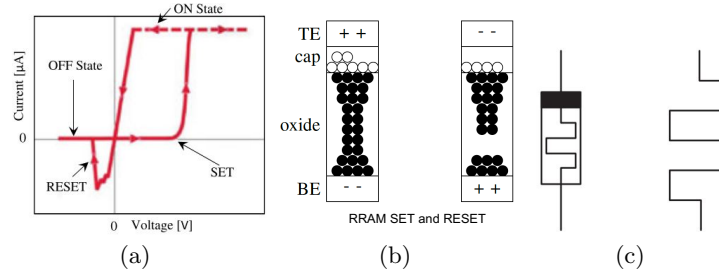


**Fig. 1.** (a) I-V characteristics of a bipolar resistive switching device [16], (b) Conductive filament in bipolar RRAM, and (c) Symbols used for representing memristive devices [18].

1(b) depicts the RRAM device including the Bottom Electrode (BE), the Top Electrode (TE) and the internal structure (metallic oxide and capping layer). When VSET is applied, the oxygen ions are attracted to the capping layer (cap) and leave behind a conductive chain of vacancies that is called a Conductive Filament (CF). However, when VRESET is applied, some of the oxygen ions move back into the oxide and rupture the CF. Fig. 1(c) shows two optional symbols used for representing memristive devices, where the black square of the left symbol represents the device's terminal for positive voltage switching [18].

Memristive devices can be initially classified into two types: (a) ionic thin film and molecular memristors, and (b) magnetic and spin-based memristor [19]. When used as memory devices, ionic thin film and molecular memristors are called resistive memories, more precisely RRAMs, being classified as a non-volatile memory [20] [19]. Note that RRAMs can be further classified as unipolar or bipolar, filamentary or area dependent switching-based, and finally according to their switching mechanism as Valence Change Mechanism (VCM), Electrochemical Mechanism (ECM) and, Thermochemical Mechanism (TCM) [17]. When considering filamentary switching, the CF is formed through the electroforming process, which is a soft breakdown phenomenon that creates a locally degraded region with a high defect concentration [20]. Note that the CF is made out of metallic impurities or oxygen vacancies, which are responsible for charge transport. Thus, filamentary, memristive VCM cells can be manufactured using different materials, such as TaOx, HfOx, and TiOx. The memristor can be manufactured on a silicon-based substrate or on a processed integrated circuit with planarized contact pads. In general terms, the memristor's fabrication includes the same basic processes, such as lithography, deposition, and etching [3, 21]. It is important to highlight that after manufacturing, especially the oxide-based filamentary-type devices, usually have a very high electrical resistance and a large voltage is required for the very first SET operation, also known as the forming process [16]. This process, a controlled soft breakdown, drastically reduces the device resistance allowing the resistance switching behavior in the subsequent cycles.

## 2.2 Defect Injection Schemes and Fault Models

The manufacturing process of memristive devices aims to create devices composed of three main parts, the BE, the Transition Metal Oxide (TMO) and finally, the TE [6]. The fabrication of memristive devices includes the same basic processes as CMOS circuits, including lithography, deposition and etching [6]. Thus, like any other device, memristors are prone to defects potentially generated during the manufacturing process due to deviations and failure mechanisms. These defects need to be properly modeled in order to guarantee an accurate identification of possible faulty behaviors of RRAM cells. Functional faults always impact the memory's functionality and can be also referred to as strong faults [22]. Contrarily, parametric faults cause parametric deviations and can be also referred to as weak faults [22]. Faults can also be further classified according to their detection conditions. In more detail, faults whose detection is guaranteed using only read and write operations, March elements, are classified as functional Easy-to-Detect (ETD) faults. They have deterministic behavior, and therefore will always lead to a logic faulty behavior that can be detected by writing into or reading from the memory cell. However, faults whose detection is not guaranteed using only read and write operations are classified as Hard-to-Detect (HTD) faults [23].

**Defect Injection Scheme:** According to literature, manufacturing defects can be injected based on the following two different models: (a) Resistive Defect (RD) model or (b) Defect Oriented (DO) model [11]. On one hand, the simulation of memristive device's faults can be done by adopting defect injection schemes based on the introduction of resistors, known as RD model. In such models, the resistance values correspond to the strength of the defects [16]. On the other hand, the simulation of a memristive device's faulty behavior can be done by altering the electrical properties of the device itself, known as DO model. It is important to highlight that all traditional and unique faults considered in this paper are modeled using the RD model.

**Conventional Fault Model:** The conventional fault model of RRAMs is composed of faults that are also observed in CMOS-based memories, such as:

- Stuck-at-Fault (SAF): the cell has its logic value stuck-at in one state, LRS or HRS [24];
- Transition Fault (TF) or Slow Write Fault (SWF): the cell fails to undergo a RESET or SET operation in the allowed time [11]. Note that the fault may occur only in one transition direction, from '1' to '0' or from '0' to '1';
- Read Disturb Fault (RDF): the cell returns a correct logic value when a read operation is performed, while the data that is stored by the cell is flipped by the read operation [11];
- Incorrect Read Fault (IRF): the cell returns an incorrect logic value when a read operation is performed, while the data stored by the cell is correct and not affected by the read operation [11];

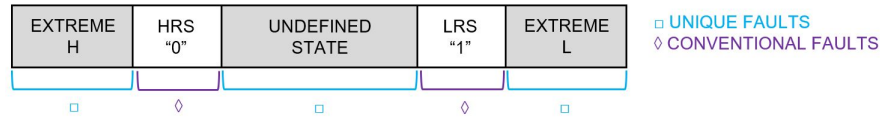


**Fig. 2.** Unique fault model: resistance intervals of faulty-free and faulty memristive devices.

- State Coupling Fault (CFst): the state of an a-cell (aggressor) impacts the data of a v-cell (victim) [25];
- Write Disturbance Fault (WDF): a write operation in a-cell changes the data in the v-cell. This fault can appear after a cycle of operations (dynamic WDF - dWDF) [26].

**Unique Fault Model** As previously mentioned, there are some exclusive faulty behaviors for RRAMs, including the following emerging faults:

- Undefined Write Fault (UWF): after a writing operation the cell is brought into an undefined state 'U' between '0' and '1', HRS and LRS [11];
- Deep State Fault (DeepF): the resistance in the cell is beyond the boundaries for each state of the cell [27];
- Unknown Read Fault (URF): the read operation results in unknown data, which means a random logic value at the output, independent from the reading conditions [11] [28]. A URF can occur when LRS and HRS are close to each other or when a state 'U' is stored in the cell. Note that the state 'U' needs to be detected because it indicates misbehavior in the memristor.

Fig. 2 depicts the faulty resistance intervals of memristive devices, where the regions highlighted in blue represent emerging faults associated to the unique fault model.

### 3 The Proposed DfT Strategy

This Section describes the proposed DfT strategy including details related to its specification as well as implementation.

#### 3.1 Specification

The DfT strategy proposed in this paper is based on the introduction of an on-chip sensor that performs electrical measurements of the RRAM cell while executing a predefined operating sequence, including READ, SET, and RESET operations. Fig. 3 depicts the general idea of how the on-chip sensor is connected to the 1T1R RRAM cell. Forward, will be proposed a DfT strategy that could be adopted on a column basis introducing just one on-chip sensor per column.



From the functional point of view, the on-chip sensor was designed to operate during the execution of READ operations only, reading the voltage between the memristor (1R) and the memristor node (MEM), and comparing this signal with an input reference voltage ( $V_{REF}$ ). Note that two control signals are used in order to activate the target resistor, which generates the correct internal reference voltage, the Voltage associated with High Resistance Reference (VHRR) or the Voltage associated to Low Resistance Reference (VLRR). A Sensor Enable (SE) signal is used in order to enable the on-chip sensor during the execution of the predefined operating sequence only, minimizing the power consumption linked with the DfT strategy's introduction. Finally, the Sensor Output (SO) indicates the result related to the comparison between the voltage at the MEM node and the internal reference voltage. Fig. 4 depicts the block diagram of the proposed on-chip sensor including the 1T1R RRAM cell. Note that was included extra hardware in order to detect DeepFs. The on-chip sensor consists of a two-stage sense amplifier [29], which compares two voltage outputs, and a set of reference resistors, named Extreme High Resistance Reference (EHRR), High Resistance Reference (HRR), Low Resistance Reference (LRR), and Extreme Low Resistance Reference (ELRR). The first resistor generates the Extreme High Reference Voltage ( $V_{REF\_EH}$ ) and the second resistor the High Reference Voltage ( $V_{REF\_H}$ ), the third, the Low Reference Voltage ( $V_{REF\_L}$ ), and finally the fourth, the Extreme Low Reference Voltage ( $V_{REF\_HL}$ ). More precisely, the sense amplifier compares the voltage of the memristor (1R) on the memristor node (MEM) with the voltage related to the set of reference resistors on the reference node (REF). Moreover, four nMOS access transistors, VEHRR, VHRR, VLRR, and VHLLRR, are used to provide a reference voltage to the REF node. This reference voltage at the REF node is obtained based on the current that flows through the set of reference resistors when applying a voltage reference at VREF.

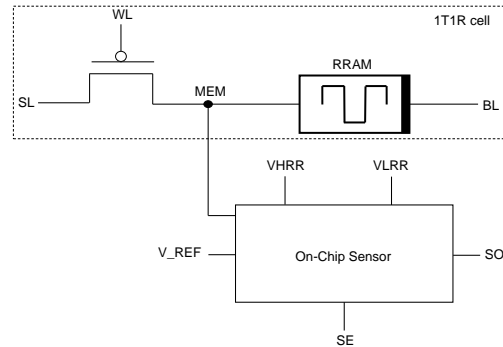


**Fig. 3.** DfT strategy: proposed on-chip sensor.

### 3.2 Implementation

The on-chip sensor proposed in this paper was implemented using a 350 nm X-FAB technology library. The selection of this particular CMOS technology node is justified by the fact that some specific size constraints for a tape-out have been posed by the group at Research Center Jülich (FZJ), Germany, that is going to manufacture the memristive devices (BEOL). Fig. 5 shows the layout of the proposed on-chip sensor. Note that the presented layout does not include the set of reference resistors (EHRR, HRR, ELRR and LRR).

The fault detection capability of the proposed methodology is guaranteed based on monitoring and comparing the voltage value of the MEM node with four distinct references (EHRR, HRR, ELRR and LRR). Note that the proposed DfT strategy was especially designed to detect the unique faults, but the on-chip sensor is also able to detect traditional faults, such as SAFs. It is important to mention that a high voltage in the MEM node is observed when a high current flows through the memristor, indicating that the memristor is in LRS or storing the value '1' ( $V_{READ\_1}$ ). Similarly, a low voltage in the MEM node is measured when a low current flows through the memristor, indicating that the memristor is in HRS or storing the value '0' ( $V_{READ\_0}$ ). Thus, the on-chip sensor compares the voltages associated to LRS and HRS with the respective reference voltages, LRR, and HRR. Note that LRR assumes a value slightly lower than LRS and HRR a value slightly higher than HRS. Fig. 6 depicts the adopted voltage levels for enabling the detection of unique faults (UWF and DeepF). The voltage associated with reading a '1' ( $V_{READ\_1}$ ) is the highest voltage to be observed in the MEM node, 1.30 V, followed by the LRR with a value of 1.16 V, the value of HRR with 1.09 V, and finally, the voltage associated to reading a '0' ( $V_{READ\_0}$ )

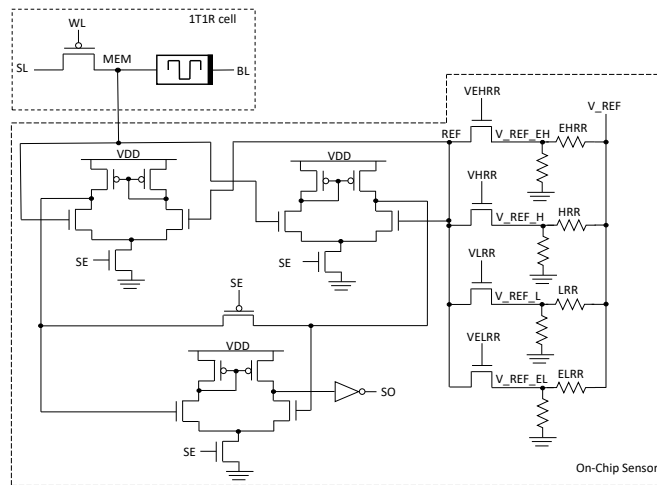
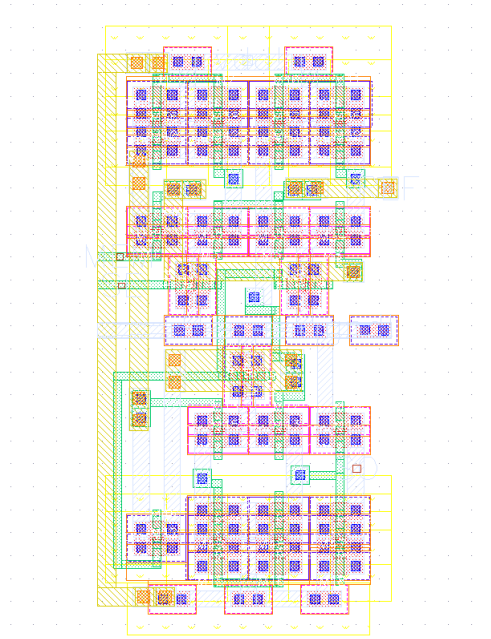


Fig. 4. Electrical schematic view of the proposed on-chip sensor.



**Fig. 5.** Layout of the designed on-chip sensor.

with 0.95 V. In order to guarantee the detection of DeepFs an extra comparison needs to be made. In this case, the extreme LRR (ELRR) was set to 1.32 V and the extreme HRR (EHRR) to 0.87 V.

Thus, when the on-chip sensor is enabled, the voltage associated to the memristor's resistance state is compared with its respective reference voltage. The results of such comparison are presented as a pulse in the SO signal, that can be stored by a latch. Fig. 7 presents implemented comparison logic. In more detail, Fig. 7 summarizes the expected values of SO when considering one traditional fault (SAF) and two unique faults (UWF and DeepF). Thus, when performing a read operation in which a '1' is expected as output, but the voltage value in the MEM node is smaller than HRR, SO is going to be '0', hence indicating that the RRAM cell presents a SAF-0. However, if the voltage at the MEM node is higher than HRR but lower than LRR, the RRAM cell assumed an undefined state 'U', indicating the occurrence of an UWF. A SAF-1 occurs when the current that flows through the memristor is higher than LRR. The DeepF Low (High) is detected when the current that flows through the memristor is higher (smaller) than ELRR (EHRR). An SO equal to '1' indicates a DeepF Low and an SO equal to '0' a DeepF High. Finally, a fault-free behavior is detected if the voltage in the MEM node is higher than LRR (SO is set to '1') or lower than HRR (SO is set to '0').

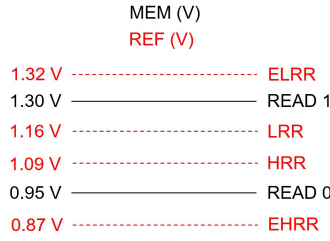


**Fig. 6.** Adopted voltage levels MEM and REF nodes: READ1/LRS, LRR, READ0/HRS, HRR, ELRR, and EHRR.

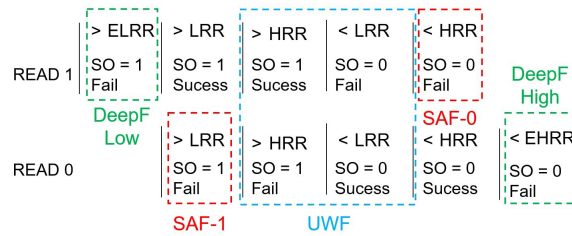


**Fig. 7.** The output of the on-chip sensor according to the performed comparisons.

It is important to point out that the detection of UWFs requires the execution of two consecutive READ operations, since the on-chip sensor has to perform two comparisons, one considering the value of HRR and another the value of LRR. However, the detection of SAFs and DeepFs can be assured performing one READ operation only. Note that the fact that the proposed on-chip sensor can detect faults from both fault models, conventional and unique, renders the solution more attractive.

## 4 Case Study and Experimental Setup

This Section presents the adopted case study and the defined experimental setup used for validating the detection capability of the proposed DFT strategy.

### 4.1 Case Study

In order to validate the proposed DfT strategy, a case study composed of a single 1T1R RRAM cell was implemented using the 350 nm X-Fab technology and the memristor model defined in [14]. Fig. 8(a) depicts the 1T1R RRAM cell and Fig. 8(b) the adopted defect injection scheme, which is based on the injection of two resistors. In this scheme, one of the resistors is in series and the other is injected in parallel with the memristor. The resistor in series ( $R_s$ ) is used for reducing the current that flows through the memristor, increasing the LRS, and consequently the voltage on the MEM node. On the contrary, the resistor in parallel ( $R_p$ )

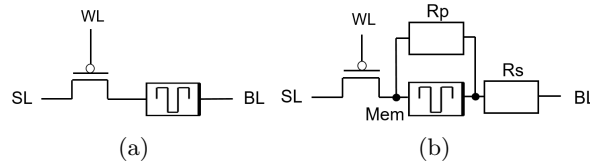


**Fig. 8.** (a) Case Study 1T1R, (b) Fault injection scheme used for the Memristor.

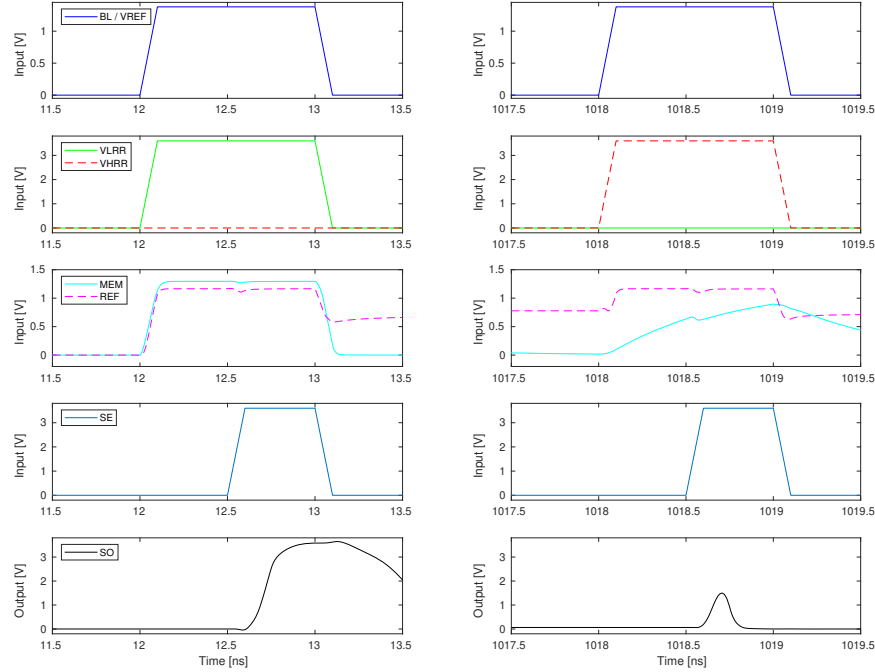
is used to increase the memristor’s current flow, decreasing the HRS, and the voltage on the MEM node. Note that the MEM node is connected to the on-chip sensor’s input and the following three signals are used to control the memristor: Bit Line (BL), Word Line (WL) and Source Line (SL).

#### 4.2 Simulation Results related to Detection Capability

To demonstrate the detection capability of the proposed DfT strategy a set of electrical simulations using SPECTRE from Cadence was performed. As previously mentioned, the adopted case study is composed of a 1T1R RRAM cell, and the on-chip sensor was connected to the MEM node between the memristor and the transistor, see Fig. 4.

In order to validate the DfT scheme, a simulation considering a defect-free RRAM cell was performed. Fig. 9 presents the behavior of the on-chip sensor when the RRAM cell is fault-free, which means that no defect was injected. Fig. 9(a) presents the sensor output when performing a read operation where the expected value is ‘1’ (LRS) and (b) when the memristor stores the value ‘0’ (HRS). The first line of the graphs presents the voltage values applied on the memristor (BL) as well as on the sensor (VREF). The second line shows the voltages used as VHRR and VLRR. The third line of the graphs shows the voltage value associated with the resistance state stored in the RRAM cell. The last two lines of the graphs depict the SE signal and the output of the sensor (SO), respectively. Thus, the graphs depicted in Fig. 9(a) show that, when SE is enabled and a read operation with an expected value of ‘1’ is executed (Read 1), the SO is high, reflecting a fault-free RRAM cell. However, when performing a read operation expecting a ‘0’, a fault free situation will be indicated by a low SO. Note that when reading a ‘1’, the reference voltage adopted is the LRR and when reading ‘0’, HRR’s value is used as reference.

The next graphs, Fig. 10, 11, 12 and 13 depict the on-chip sensor’s behavior when injecting defects (Rs and Rp) able to cause the following faults: SAF-0, SAF-1, UWF, DeepF High as well as DeepF Low. Although the on-chip sensor was not specifically developed for detecting traditional faults affecting RRAMs, since the main goal of the proposed DfT was to guarantee the detection of unique faults, the proposed approach is also able to detect traditional faults, such as SAFs. The detection of SAF-0 occurs when the current that flows through the memristor is lower than the expected one, see Fig. 10(a). In that case, the on-chip sensor compares the voltage value at the MEM node with HRR and sets



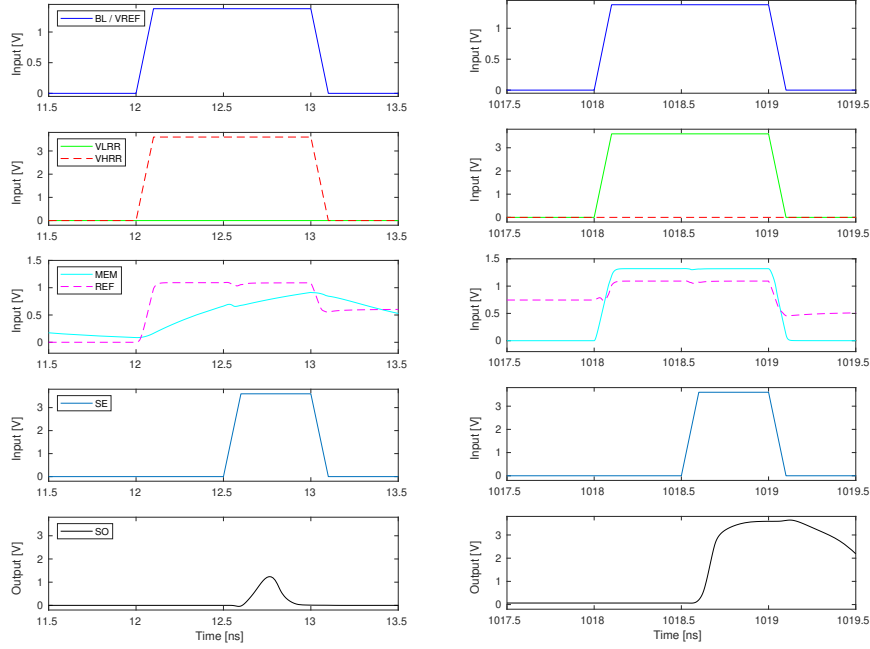
(a) Read 1 &gt; LRR, SO = 1.

(b) Read 0 &lt; HRR, SO = 0.

**Fig. 9.** Validation of the on-chip sensor considering fault free RRAM cell.

the SO signal to low. Note that in order to model a SAF-0,  $R_s$  was set to  $70\text{ k}\Omega$ . Fig. 10(b) depicts the results associated with the injection of a defect that was modeled by setting  $R_p$  equal to  $1\text{ k}\Omega$ . The graph in 10(b) shows the detection of a SAF-1, since the expected output of the performed read operation was '0'. Note that the detection of SAF-1 is indicated by setting SO to high.

Fig. 11 and 12 demonstrate the proposed on-chip sensor's detection capability with respect to UWFs. As previously mentioned, the detection of these faults requires the execution of two consecutive read operations, since two comparisons are required (one with HRR and another with LRR). Two different simulations were performed, one injecting a defect using an  $R_s$  set to  $15\text{ k}\Omega$  (a read operation of '1') and another using an  $R_p$  with  $30\text{ k}\Omega$  (a read operation of '0'). Observing the graphs in Fig. 11 it is possible to see that the on-chip sensor was able to detect the UWF when *Read1* is performed since SO was set to low when comparing the value of MEM node to LRR and set to high when compared to HRR. The detection of the UWF when performing a read operation with an expected output of '0' is depicted in Fig. 12. In that case, SO is set to low when compared to LRR



(a) SAF-0: Read 1 < HRR, SO = 0. (b) SAF-1: Read 0 > LRR, SO = 1.

**Fig. 10.** On-chip sensor detection capability: SAFs.

and to high when compared to HRR. Note again that the detection of UWFs is only possible by executing two comparisons. When considering a read operation expecting a '1', the faulty behavior is detected when the voltage at the MEM node is both smaller than LRR and bigger than HRR.

Fig. 13 shows the on-chip sensor's detection capability with respect to DeepFs. Note that the detection of these unique faults requires one read operation only, and the signals in the second line now show the voltages VEHRR and VELRR. The DeepF Low was modeled injecting an  $R_p$  of  $500 \Omega$  and the Deep High an  $R_s$  of  $1 M\Omega$ . Observing the graphs depicted in Fig. 13 it is possible to see that a read operation expecting a '1' is performed in order to detect a DeepF Low. The SO is set to '1' when the voltage at the MEM node is bigger than ELRR. However, a DeepF High is detected when the voltage at the MEM node is smaller than EHRR. The detection of a Deep High is indicated by a SO equal to '0'.

Finally, it is important to mention that the DfT strategy is also able to provide the detection of the other faults associated with the RRAM conventional fault model, such as TF and RDF. The simulation results related to these traditional faults were omitted because the main goal of this Section is to demonstrate

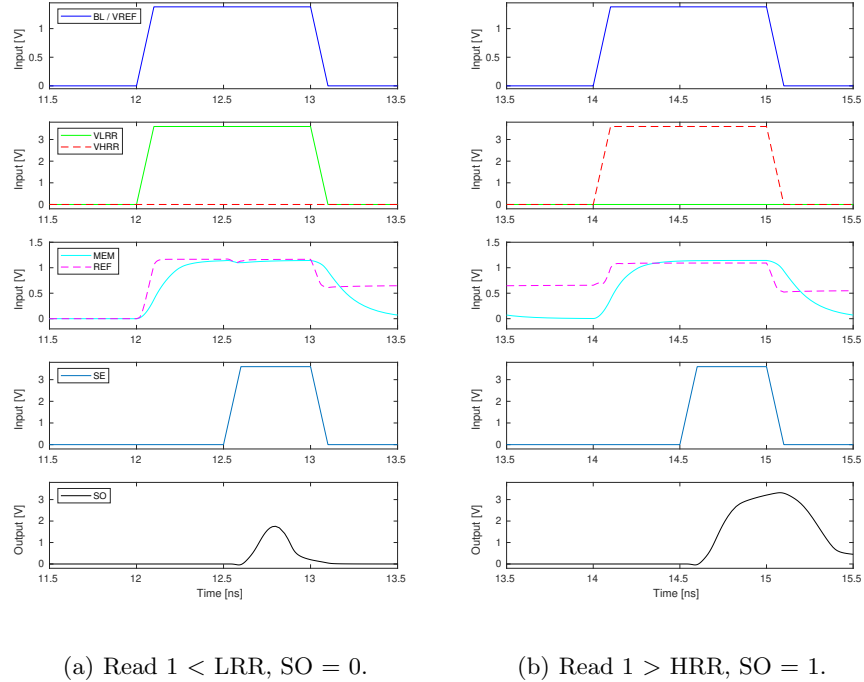


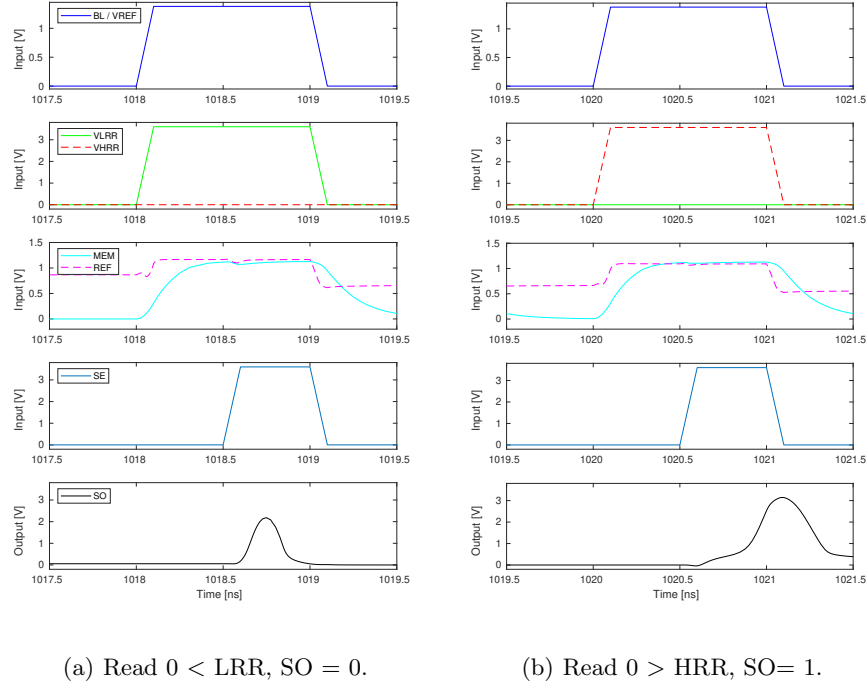
**Fig. 11.** On-chip sensor detection capability when performing a read operation expecting '1': UWF.

the detection capability of the proposed approach with respect to unique faults only since their detection represents the most important challenge when dealing with RRAMs.

### 4.3 Discussion about introduced overheads and implementation granularity

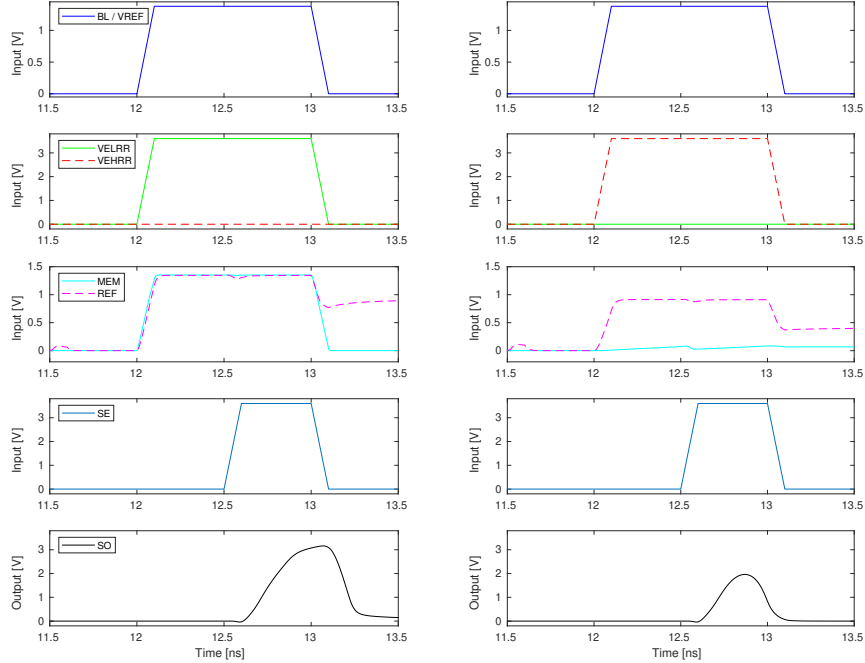
The proposed DfT approach introduces an area overhead that is not observed when using software-based manufacturing test procedures, such as March Tests. However, March Tests can not guarantee the detection of all unique faults in RRAMs. It is important to highlight that memory faults can be classified as strong or weak faults [10]. Strong faults are functional faults that can always be sensitized by applying a sequence of write and read operations. In contrast, weak faults cause parametric faults and can not be detected with any sequence of write and read operations, since they do not cause functional errors. These faults, when not detected after manufacturing, may become a reliability issue during their lifetime. Thus, as previously mentioned, depending on the effort needed to detect faults caused by manufacturing defects, these faults can be





**Fig. 12.** On-chip sensor detection capability when performing a read operation expecting '0': UWF.

further categorized into ETD and HTD faults. Note that strong faults consist of ETD and HTD faults, while weak faults are all HTD. To resume, the proposed DfT approach is able to provide the detection of HTD faults, which justifies the introduced area overhead. The area of the proposed on-chip sensor is around  $278 \mu\text{m}^2$ , assuming the technology node adopted in this work (350 nm X-Fab technology). Note that this value does not include the transistors related to the reference voltages. In order to understand the area impact related to the introduction of the proposed DfT strategy, it is important to mention that the area associated to a 1T1R RRAM cell is around  $40 \mu\text{m}^2$  for the transistor and the memristor can have an area of around  $50 \mu\text{m}^2$ , when fabricated based on the Microcrossbar technology, or  $0.1 \mu\text{m}^2$  if using the Nano-crossbar technology. This area overhead could be considered relevant with respect to a 1T1R RRAM cell. However, the overhead becomes irrelevant when considering a complete RRAM composed including the 1T1R cell array as well as all peripheral circuitry. Figure 14 depicts one possible implementation of the proposed DfT strategy, where one on-chip sensor is connected to each column of the RRAM block. In more detail, the on-chip sensor could be connected to the Source Line (SL) of the block. During a read operation, the on-chip sensor compares the current of the

(a) Read  $1 > ELRR$ ,  $SO = 1$ .(b) Read  $0 < EHRR$ ,  $SO = 0$ .**Fig. 13.** On-chip sensor detection capability to detect DeepFs

1T1R RRAM cell column with the two reference voltages, the  $V_{REF\_H}$  and the  $V_{REF\_L}$ . Thus, based on this comparison, the on-chip sensor identifies the resistive state associated with the current that flows through the 1T1R RRAM cell column. A possible limitation of this implementation granularity is associated to the on-chip sensor resolution, since depending on the CMOS technology node, the on-chip sensor could be susceptible to process variation, impacting its ability to properly indicate a faulty behavior. Note that in order to assume this granularity, the on-chip sensor needs to measure the current consumption, instead of the voltage. Another important point to be considered is related to the power overhead. The on-chip sensor has a power consumption of around 2.4 mW, while the 1T1R RRAM cell consumes approximately 1.76 mW during the SET operation and  $2.2 \mu\text{W}$  during the RESET operation. Note that in order to reduce the power overhead introduced by the proposed approach, the on-chip sensor is only enabled when used, which means during the execution of read operations included in the predefined operating sequence only. Finally, it is important to highlight that the DfT strategy significantly reduces the time re-

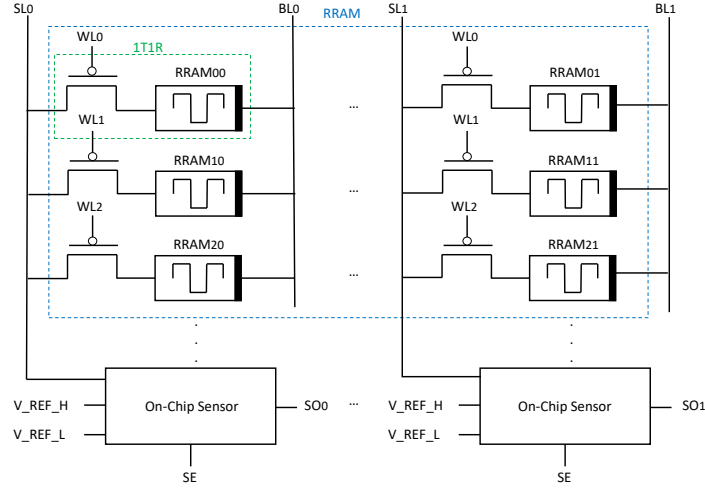


Fig. 14. Electrical schematic view of the proposed on-chip sensor in the block.

quired for performing the manufacturing test with respect to March Tests, since the operating sequence applied in combination with the electrical measurements is significantly smaller.

## 5 Final Remarks

The use of RRAMs to replace classic CMOS-based memories represents an interesting alternative in order to guarantee the storage of high data volumes as well as implement emerging applications. However, aspects regarding their quality after manufacturing are still a challenge, since functional test algorithms cannot guarantee the detection of unique faults, which are classified as HTD faults. This paper presents a DfT strategy able to detect traditional and unique faults caused by manufacturing deviations in RRAMs. The proposed strategy consists of introducing an on-chip sensor able to compare the voltage associated with HRS and LRS with a set of predefined reference voltages while executing a predefined operating sequence. This set is composed of at least two resistors, representing the reference voltage associated with HRS and LRS. The results obtained through electrical simulations demonstrate the fault detection capability of the proposed DfT strategy. When compared to state-of-the-art solutions, the DfT strategy has the advantage of detecting not only traditional faults but also all unique faults that can affect RRAMs. The introduced area overhead can be minimized and become tolerable when assuming an implementation granularity considering one on-chip sensor per each RRAM column. Finally, the power consumption of the proposed on-chip sensor does not represent a significant overhead when considering the power associated with a 1T1R RRAM cell executing SET and RESET operations.

## Acknowledgment

This work was supported by the Federal Ministry of Education and Research (BMBF, Germany) within the NEUROTEC I II projects 16ES1134 and 16ME0399.

## References

1. G. M. Moore, "Cramming more components onto integrated circuits With unit cost," *Electronics*, vol. 38, no. 8, p. 114, 1965. [Online]. Available: <https://newsroom.intel.com/wp-content/uploads/sites/11/2018/05/moores-law-electronics.pdf>
2. R. Dennard, F. Gaensslen, W.-N. Yu, L. Rideout, E. Bassous, and A. Le Blanc, "Design of Ion-Implanted Small MOSFET ' S Dimensions with Very," *IEEE Journal of Solid State Circuits*, vol. 9, no. 5, pp. 257–268, 1974.
3. S. Hamdioui, S. Kvatinsky, G. Cauwenberghs, L. Xie, N. Wald, S. Joshi, H. M. Elsayed, H. Corporaal, and K. Bertels, "Memristor for computing: Myth or reality?" in *Proceedings of the 2017 Design, Automation and Test in Europe, DATE 2017*. Institute of Electrical and Electronics Engineers Inc., may 2017, pp. 722–731.
4. P. Mazumder, S. M. Kang, and R. Waser, "Memristors: Devices, models, and applications," in *Proceedings of the IEEE*, vol. 100, no. 6, jun 2012, pp. 1911–1919.
5. A. Chaudhuri and K. Chakrabarty, "Analysis of process variations, defects, and design-induced coupling in memristors," in *2018 IEEE International Test Conference (ITC)*, 2018, pp. 1–10.
6. L. M. B. Poehls, M. C. R. Fieback, S. Hoffmann-Eifert, T. Copetti, E. Brum, S. Menzel, S. Hamdioui, and T. Gemmeke, "Review of Manufacturing Process Defects and Their Effects on Memristive Devices," *Journal of Electronic Testing*, vol. 37, no. 4, pp. 427–437, 2021. [Online]. Available: <https://doi.org/10.1007/s10836-021-05968-8>
7. S. Hamdioui, M. Taouil, and N. Z. Haron, "Testing open defects in memristor-based memories," *IEEE Transactions on Computers*, vol. 64, no. 1, pp. 247–259, 2015.
8. N. Z. Haron and S. Hamdioui, "Dft schemes for resistive open defects in rrams," in *2012 Design, Automation & Test in Europe Conference & Exhibition (DATE)*. IEEE, 2012, pp. 799–804.
9. S. Hamdioui, M. Taouil, and N. Z. Haron, "Testing open defects in memristor-based memories," *IEEE Transactions on Computers*, vol. 64, no. 1, pp. 247–259, 2013.
10. M. Fieback, L. Wu, G. C. Medeiros, H. Aziza, S. Rao, E. J. Marinissen, M. Taouil, and S. Hamdioui, "Device-aware test: A new test approach towards DPPB level," in *Proceedings - International Test Conference*, vol. 2019-Novem, 2019.
11. M. Fieback, M. Taouil, and S. Hamdioui, "Testing resistive memories: Where are we and what is missing?" in *2018 IEEE International Test Conference (ITC)*, 2018, pp. 1–9.
12. S. Kannan, J. Rajendran, R. Karri, and O. Sinanoglu, "Sneak-path testing of crossbar-based nonvolatile random access memories," *IEEE Transactions on Nanotechnology*, vol. 12, no. 3, pp. 413–426, 2013.

13. T. S. Copetti, T. Gemmeke, and L. M. Bolzani Poehls, "Validating a dfT strategy's detection capability regarding emerging faults in rrams," in *2021 IFIP/IEEE 29th International Conference on Very Large Scale Integration (VLSI-SoC)*, 2021, pp. 1–6.
14. "Jart vcm v1b," <http://www.emrl.de/JART.html>, accessed: 2021-04-11.
15. L. Chua, "Memristor - The Missing Current Element," *IEEE Transactions on Circuit Theory*, vol. CT-18, no. No. 5, 1971.
16. E. I. Vatajelu, P. Prinetto, M. Taouil, and S. Hamdioui, "Challenges and solutions in emerging memory testing," *IEEE Transactions on Emerging Topics in Computing*, vol. 7, no. 3, pp. 493–506, 2017.
17. R. Waser, "Electrochemical and thermochemical memories," in *Technical Digest - International Electron Devices Meeting, IEDM*, 2008.
18. J. Yu, H. A. Du Nguyen, L. Xie, M. Taouil, and S. Hamdioui, "Memristive devices for computation-in-memory," in *2018 Design, Automation & Test in Europe Conference & Exhibition (DATE)*. IEEE, 2018, pp. 1646–1651.
19. D. Ielmini and V. Milo, "Physics-based modeling approaches of resistive switching devices for memory and in-memory computing applications," *Journal of Computational Electronics*, vol. 16, no. 4, pp. 1121–1143, 2017.
20. R. Waser, R. Dittmann, C. Staikov, and K. Szot, "Redox-based resistive switching memories nanoionic mechanisms, prospects, and challenges," *Advanced Materials*, vol. 21, no. 25-26, pp. 2632–2663, 2009.
21. A. Hardtdegen, C. La Torre, F. Cuppers, S. Menzel, R. Waser, and S. Hoffmann-Eifert, "Improved switching stability and the effect of an internal series resistor in HfO<sub>2</sub>/TiO<sub>x</sub> Bilayer ReRAM Cells," *IEEE Transactions on Electron Devices*, vol. 65, no. 8, pp. 3229–3236, aug 2018.
22. G. Cardoso Medeiros, M. Fieback, L. Wu, M. Taouil, L. M. Bolzani Poehls, and S. Hamdioui, "Hard-to-detect fault analysis in finfet srams," *IEEE Transactions on Very Large Scale Integration (VLSI) Systems*, vol. 29, no. 6, pp. 1271–1284, 2021.
23. S. Arvindam, V. Kumar, V. Nageshwara Rao, and V. Singh, "Automatic test pattern generation on multiprocessors: a summary of results," in *International Conference on Knowledge Based Computer Systems*. Springer, 1989, pp. 39–51.
24. N. Z. Haron and S. Hamdioui, "On defect oriented testing for hybrid cmos/memristor memory," in *2011 Asian Test Symposium*. IEEE, 2011, pp. 353–358.
25. C.-Y. Chen, H.-C. Shih, C.-W. Wu, C.-H. Lin, P.-F. Chiu, S.-S. Sheu, and F. T. Chen, "Rram defect modeling and failure analysis based on march test and a novel squeeze-search scheme," *IEEE Transactions on Computers*, vol. 64, no. 1, pp. 180–190, 2014.
26. Y.-X. Chen and J.-F. Li, "Fault modeling and testing of 1t1r memristor memories," in *2015 IEEE 33rd VLSI Test Symposium (VTS)*. IEEE, 2015, pp. 1–6.
27. S. Kannan, J. Rajendran, R. Karri, and O. Sinanoglu, "Sneak-path testing of memristor-based memories," in *2013 26th International Conference on VLSI Design and 2013 12th International Conference on Embedded Systems*. IEEE, 2013, pp. 386–391.
28. —, "Sneak-path testing of crossbar-based nonvolatile random access memories," *IEEE Transactions on Nanotechnology*, vol. 12, no. 3, pp. 413–426, 2013.
29. J. M. Rabaey, A. P. Chandrakasan, and B. Nikolić, *Digital integrated circuits: a design perspective*. Pearson education Upper Saddle River, NJ, 2003, vol. 7.